Numer. Math. Theor. Meth. Appl.
doi: 10.4208/nmtma.OA-2020-0023

Published online 9 October 2020

Phase-Field Modeling and Numerical Simulation for Ice Melting

Jian Wang[1], Chaeyoung Lee[2], Hyun Geun Lee[3], Qimeng Zhang[4], Junxiang Yang[2], Sungha Yoon[2], Jintae Park[2] and Junseok Kim[2,*]

[1] *School of Mathematics and Statistics, Nanjing University of Information Science and Technology, Nanjing, 210044, China*
[2] *Department of Mathematics, Korea University, Seoul 02841, Republic of Korea*
[3] *Department of Mathematics, Kwangwoon University, Seoul 01897, Republic of Korea*
[4] *Interdisciplinary Program in Visual Information Processing, Korea University, Seoul 02841, Republic of Korea*

Received 7 February 2020 ; Accepted (in revised version) 27 August 2020

Abstract. In this paper, we propose a mathematical model and present numerical simulations for ice melting phenomena. The model is based on the phase-field modeling for the crystal growth. To model ice melting, we ignore anisotropy in the crystal growth model and introduce a new melting term. The numerical solution algorithm is a hybrid method which uses both the analytic and numerical solutions. We perform various computational experiments. The computational results confirm the accuracy and efficiency of the proposed method for ice melting.

AMS subject classifications: 65M06, 65D17, 68U05, 68U07, 93A30

Key words: Allen-Cahn equation, phase-field model, ice melting.

1. Introduction

Melting is an important problem which is associated to various engineering field such as electroslag melting, welding and thawing of moist soil. Melting is the process of heating a substance to change it from solid to liquid, which is a common type of state change. Heat transfer is a physical phenomenon in physics, which refers to the phenomenon of heat transfer caused by temperature difference. Some melting models of heat transfer have been proposed in the past decades [20, 31, 40, 41, 45]. In [24], the authors applied a melting model based on the enthalpy-porosity method

*Corresponding author. *Email address:* cfdkim@korea.ac.kr (J.S. Kim)

to investigate the effects of porosity on the ice melting process and heat transfer. Experimental results for the characterisation of the freezing and melting processes for water contained in spherical ice thermal storage elements were described and evaluated [10]. Three-dimensional melting of ice around a liquid-carrying tube placed in an adiabatic rectangular cavity was investigated by numerical analysis [39]. Fujishiro and Aoki [13] presented volume modeling of the phenomenon by mathematical morphology and cellular automaton using voxels to represent ice objects and calculated the heat conduction and melting effects based on volume operation. Zheng [49] used a lattice Boltzmann method with an interfacial tracking method to solve melting problem in an enclosure. Jones presented a method for animating melting solids and proposed a method to simulate the melting process taking account of the thermal flow and the latent heat caused by the phase change [19]. For animating materials that melt, flow, and solidify, Carlson presented a fast and stable system and simulated the melting of solids such as waxes by treating solids as fluids with very high viscosities [5]. Melting and flowing behaviors were simulated by solving the Navier-Stokes equations. Although this method can simulate the melting and flowing of high viscosity materials, it is not applicable to simulations of ice melting because the viscosity of water is low. Paiva *et al.* proposed a physical simulation for melting viscoplastic objects [32].

In addition, some works presented the melting phenomena with a perspective of computational vision [12, 15, 26, 28, 38, 48]. In this study, we focus on ice melting by using a mathematical modeling. We propose a model to investigate the ice melting with the modified Allen-Cahn (AC) equation [1, 8]. In the proposed model, the temperature field is added to model the phenomenon of heat transfer for ice melting. Furthermore, we analyze the physical phenomenon of the ice cubes with different shapes. The proposed model is based on the phase-field method. The most significant computational advantage of the phase-field method is that an explicit tracking of the interface is unnecessary [11]. In a sharp interface method, it is necessary to solve highly coupled equations to track the evolution of individual interfaces during transformation [33]. In the phase-field method, however, we can describe the evolution of the phase-field with relatively simple equations involving mass and heat changes. As the reverse process of ice melting, the phenomena of crystal growth have been widely simulated by using a phase-field model [3,7,18,34,43]. However, there is little investigation for ice melting such as the melting process from ice to water. Therefore, we propose a mathematical modeling and present numerical simulations for ice melting in this paper.

The contents of this paper are as follows. In Section 2, we present a phase-field model for ice melting based on the modified AC equation. In Section 3, we describe a robust hybrid numerical method for the proposed model. In Section 4, we perform numerical experiments. Finally, we conclude in Section 5.

2. The phase-field model

We propose a phase-field method [29, 35] for ice melting simulation. We introduce a phase-field $\phi(\mathbf{x}, t)$ whose value is close to 1 if $\mathbf{x}$ is in the ice and is close to -1 if $\mathbf{x}$

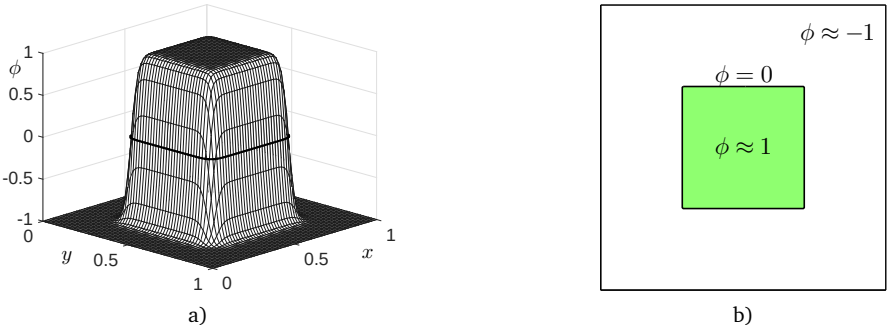

a) b)

Figure 1: a) Shape of the phase-field function ϕ. b) Contour of ϕ at the zero level.

is in the liquid at time t. In addition, we have the temperature field $U(\mathbf{x}, t) = 0$ and $U(\mathbf{x}, t) = 1$ in the model, corresponding to ice and liquid, respectively. Due to the heat transfer, the phase-field $\phi(\mathbf{x}, t)$ of ice changes from 1 to -1, which results in the temperature field $U(\mathbf{x}, t)$ of the liquid decreases from 1. Fig. 1 shows a rectangular ice and we interpret the zero level set of the phase-field as the interface between ice and liquid.

The anisotropic form of the phase-field equation for the solidification is given by

$$\epsilon^2(\phi)\frac{\partial \phi}{\partial t} = \nabla\left(\epsilon^2(\phi)\nabla\phi\right) + \left[\phi - \lambda U(1-\phi^2)\right]\left(1-\phi^2\right) + \left(|\Delta\phi|^2\,\epsilon(\phi)\frac{\partial \epsilon(\phi)}{\partial \phi_x}\right)_x + \left(|\Delta\phi|^2\,\epsilon(\phi)\frac{\partial \epsilon(\phi)}{\partial \phi_y}\right)_y + \left(|\Delta\phi|^2\,\epsilon(\phi)\frac{\partial \epsilon(\phi)}{\partial \phi_z}\right)_z, \tag{2.1}$$

$$\frac{\partial U}{\partial t} = D\Delta U - \frac{1}{2}\frac{\partial \phi}{\partial t}, \tag{2.2}$$

where ϕ is the order parameter and $\epsilon(\phi)$ is the anisotropic function [25]. The order parameter is defined by $\phi \approx 1$ in the solid phase and $\phi \approx -1$ in the liquid phase. The interface is defined by $\phi = 0$. λ is the dimensionless coupling parameter, U is the dimensionless temperature field, and D is the thermal diffusivity. In Fig. 2, we can see the crystal growth using a phase-field equation [46].

If the crystal growth process is isotropic, then $\epsilon(\phi)$ is constant, i.e., $\epsilon(\phi) = \epsilon$ and Eq. (2.1) becomes

$$\frac{\partial \phi}{\partial t} = \Delta\phi - \frac{1}{\epsilon^2}\left(\phi^3 - \phi\right) - \frac{1}{\epsilon^2}\lambda U\left(1-\phi^2\right)^2, \tag{2.3}$$

which is the AC equation with a nonlinear source term.

Based on this observation, we propose a phase-field equation for modeling ice melting by ignoring the anisotropic interfacial energy and adding a melting term. According to [22], we can easily get our energy functional as

$$\mathscr{W} = \int_\Omega \left[\frac{M}{2}|\nabla\phi|^2 + M\frac{F(\phi)}{\epsilon^2} + \lambda U\frac{\phi - (1/3)\phi^3}{\sqrt{2}\epsilon}\right] d\mathbf{x}. \tag{2.4}$$

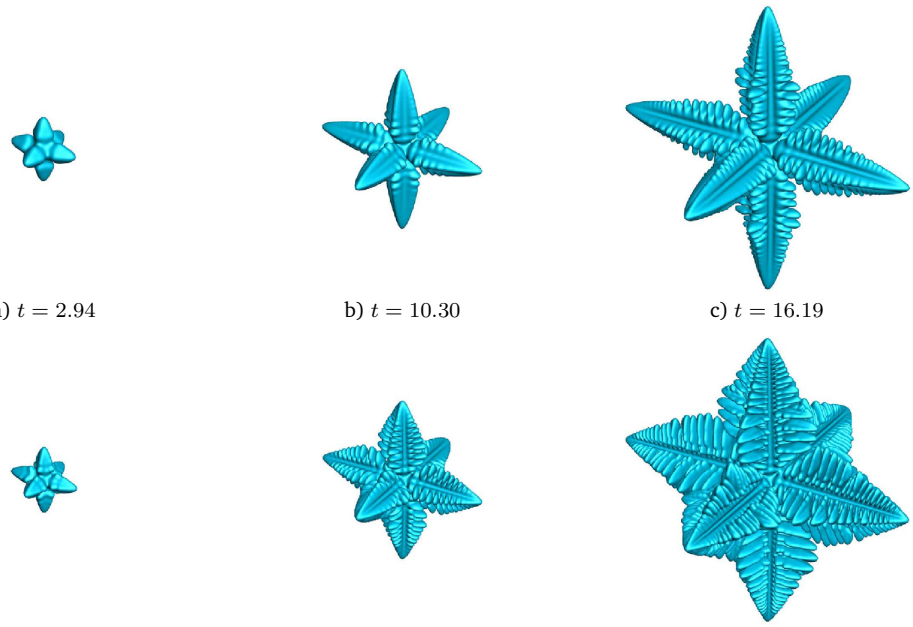

a) $t = 2.94$ b) $t = 10.30$ c) $t = 16.19$

d) $t = 2.94$ e) $t = 5.89$ f) $t = 8.83$

Figure 2: Crystal growth under undercooling of 4Kelvin and 6Kelvin for the top and the bottom rows, respectively. Reprinted from Yang *et al.* [46] with permission from the Elsevier.

Then,

$$\frac{\delta \mathscr{W}}{\delta \phi} = -M\Delta\phi + M\frac{F'(\phi)}{\epsilon^2} + \lambda U\frac{1-\phi^2}{\sqrt{2}\epsilon}, \tag{2.5}$$

where $\frac{\delta}{\delta\phi}$ denotes the variational derivative with respect to ϕ and $F(\phi) = 0.25(\phi^2-1)^2$ is a double well potential energy [9] (see Fig. 3). Here, M is a constant mobility. Following Jacqmin and Ceniceros *et al.* [6,16], we take $M = \mathcal{O}(\epsilon)$, where the parameter ϵ is a measure of interface thickness.

Therefore, we have

$$\frac{\partial \phi}{\partial t} = -\frac{\delta \mathscr{W}}{\delta \phi} = M\left(\Delta\phi - \frac{F'(\phi)}{\epsilon^2}\right) - \lambda U\frac{\sqrt{2F(\phi)}}{\epsilon}, \tag{2.6}$$

$$\frac{\partial U}{\partial t} = D\Delta U - \frac{1}{2}\frac{\partial \phi}{\partial t}. \tag{2.7}$$

In Eq. (2.6), we use the form $\sqrt{2F(\phi)}/\epsilon$ to give the melting effect on interfacial transition region, $|\nabla\phi| \neq 0$, because the phase-field ϕ at the equilibrium state satisfies $F(\phi) = 0.5\epsilon^2|\nabla\phi|^2$ [17, 23]. The phase-field ϕ in the ice can be less than 1 because of the source term in Eq. (2.6). Then, the form $4F(\phi)/\epsilon^2$ allows melting inside the ice. Therefore, the melting effect only at the interfacial region was given by using the term

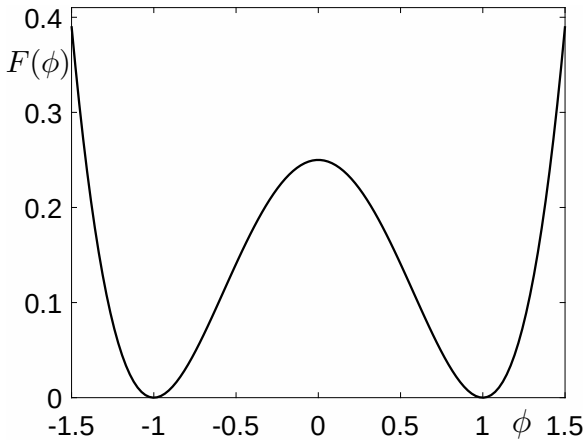

Figure 3: A double well potential, $F(\phi) = 0.25(\phi^2 - 1)^2$.

$|\nabla\phi| = \sqrt{2F(\phi)}/\epsilon$. By differentiation of the total energy $\mathscr{W}(\phi)$,

$$\frac{d}{dt}\mathscr{W}(\phi) = \int_\Omega \frac{\delta\mathscr{W}}{\delta\phi}\frac{\partial\phi}{\partial t}d\mathrm{x} = \int_\Omega \left(-\frac{\partial\phi}{\partial t}\right)\frac{\partial\phi}{\partial t}d\mathrm{x} = -\int_\Omega \left(\frac{\partial\phi}{\partial t}\right)^2 d\mathrm{x} \leq 0. \tag{2.8}$$

Thus, we can see that the total energy decreases with t. The term $-\lambda U\sqrt{2F(\phi)}/\epsilon$ models melting in this paper and its detailed derivation for evaporation phenomenon will be published elsewhere. For the interested readers, we briefly describe the derivation of the melting term under the constant ambient temperature. We consider a spherical ice with radius R. Let $V = \frac{4\pi R^3}{3}$ and $S = 4\pi R^2$ be its volume and surface area, respectively, and we assume that the melting rate $\frac{dV}{dt}$ is proportional to S, i.e.,

$$\frac{dV}{dt} = -\lambda S, \tag{2.9}$$

where λ is a melting rate constant. Then, Eq. (2.9) becomes $\frac{dR}{dt} = -\lambda$ and its solution is $R(t) = R_0 - \lambda t$, where R_0 is an initial radius of the spherical ice. Let us consider a profile,

$$\phi(R,t) = \tanh\left(\frac{R_0 - R - \lambda t}{\sqrt{2}\epsilon}\right). \tag{2.10}$$

Then, differentiating Eq. (2.10) with respect to time variable t yields

$$\begin{aligned}\frac{\partial\phi(R,t)}{\partial t} &= -\frac{\lambda}{\sqrt{2}\epsilon}\mathrm{sech}^2\left(\frac{R_0 - R - \lambda t}{\sqrt{2}\epsilon}\right)\\ &= -\frac{\lambda}{\sqrt{2}\epsilon}\left(1 - \tanh^2\left(\frac{R_0 - R - \lambda t}{\sqrt{2}\epsilon}\right)\right)\\ &= -\frac{\lambda}{\sqrt{2}\epsilon}\left(1 - \phi^2(R,t)\right) = -\frac{\lambda}{\epsilon}\sqrt{2F(\phi(R,t))}.\end{aligned} \tag{2.11}$$

Finally, we multiply the temperature U to the right hand side of Eq. (2.11) to get the melting term.

3. Numerical solution

In this section, we propose a robust hybrid numerical method for ice melting simulation. Let $\Omega = (-a, a) \times (-b, b) \times (-c, c)$ be the computational domain. Let N_x, N_y, and N_z be positive even integers, $h = \frac{2a}{N_x} = \frac{2b}{N_y} = \frac{2c}{N_z}$ be the uniform mesh size, and

$$\begin{aligned}\Omega_h = &\big\{(x_i, y_j, z_k) : x_i = -a + (i - 0.5)h, y_j = -b + (j - 0.5)h,\\ &z_k = -c + (k - 0.5)h, 1 \le i \le N_x, 1 \le j \le N_y, 1 \le k \le N_z\big\}\end{aligned}$$

be the set of cell-centers. Let ϕ^n_{ijk} and U^n_{ijk} be approximations of $\phi(x_i, y_j, z_k, n\Delta t)$ and $U(x_i, y_j, z_k, n\Delta t)$, where $\Delta t = \frac{T}{N_t}$ is the time step, T is the final time, and N_t is the total number of time steps. For a numerical solution of the governing equations, there are various methods [14, 27, 37, 44, 47]. In this paper, we use a Crank-Nicolson type scheme for Eqs. (2.6) and (2.7):

$$\begin{aligned}\frac{1}{\Delta t}\Big(\phi^{n+1}_{ijk} - \phi^n_{ijk}\Big) = \frac{M}{2}\left(\Delta_d\phi^{n+1}_{ijk} - \frac{1}{\epsilon^2}F'\big(\phi^{n+1}_{ijk}\big) + \Delta_d\phi^n_{ijk} - \frac{1}{\epsilon^2}F'\big(\phi^n_{ijk}\big)\right)\\ - \frac{\lambda}{2\epsilon}\left(3U^n_{ijk} - U^{n-1}_{ijk}\right)\sqrt{2F\left(0.5\big(3\phi^n_{ijk} - \phi^{n-1}_{ijk}\big)\right)}, \qquad (3.1)\end{aligned}$$

$$\frac{1}{\Delta t}\Big(U^{n+1}_{ijk} - U^n_{ijk}\Big) = \frac{D}{2}\Delta_d\left(U^{n+1}_{ijk} + U^n_{ijk}\right) - \frac{1}{2\Delta t}\Big(\phi^{n+1}_{ijk} - \phi^n_{ijk}\Big), \qquad (3.2)$$

where Δ_d is the standard discrete Laplacian operator, defined as

$$\Delta_d\phi_{ijk} = \frac{1}{h^2}\big(\phi_{i-1,jk} + \phi_{i+1,jk} + \phi_{i,j-1,k} + \phi_{i,j+1,k} + \phi_{ij,k-1} + \phi_{ij,k+1} - 6\phi_{ijk}\big).$$

We use homogeneous Neumann boundary conditions [30] for ϕ and U for simplicity. We set the initial settings $\phi^{-1}_{ijk} = \phi^0_{ijk}$ and $U^{-1}_{ijk} = U^0_{ijk}$. The first order temporal accuracy due to the first time step reduction does not affect the overall second order accuracy of the numerical scheme [36], as shown in Section 4.1. We solve the discrete equations (3.1) and (3.2) using a multigrid method [2, 42].

4. Computational results

In this section, we present numerical results using the proposed phase-field model. Before we start, we define the interfacial length parameter ϵ_m as

$$\epsilon_m = \frac{mh}{2\sqrt{2}\tanh^{-1}(0.9)},$$

which implies that we have approximately mh transition layer width [21]. For all tests, we use $\epsilon = \epsilon_m$ for some integer m, unless otherwise specified.

4.1. Convergence test

We first present the convergence rates of the numerical scheme for the phase-field ϕ and temperature field U as the mesh size h gets refined. The initial condition of a sphere is given by

$$\phi(x,y,z,0) = \tanh\left(\frac{R_0 - R}{\sqrt{2}\epsilon}\right),$$

where $R = \sqrt{x^2+y^2+z^2}$ and the initial radius $R_0 = 35$ on a computational domain $\Omega = (-50,50)^3$. We take the initial condition of temperature as $U(x,y,z,0) = 0.5(1 - \phi(x,y,z,0))$. We perform the convergence tests on the uniform grids, $h = \frac{100}{N_h}$ for $N_h = 16, 32, 64, 128$, which is the number of grid points in each axis with respect to h. The time step size is fixed at $\Delta t = 0.03$ and the final time is $T = 5\Delta t$. We use the parameters such as $\epsilon = 20, M = 10\epsilon, \lambda = 5$, and $D = 1$. We define the discrete l_2-norm of relative error to the space as follows:

$$\left\|e^{h,\frac{h}{2}}\right\|_2 = \sqrt{\frac{1}{N_h^3}\sum_{i,j,k}\left(e_{ijk}^{h,\frac{h}{2}}\right)^2}, \tag{4.1}$$

where $e_{ijk}^{h,\frac{h}{2}}$ is an absolute error between values of coarse and of fine grids defined as

$$\begin{aligned} e_{ijk}^{h,\frac{h}{2}} = \Big|\phi_{ijk}^{n,h} - 0.125\Big(&\phi_{2i-1,2j-1,2k-1}^{n,\frac{h}{2}} + \phi_{2i-1,2j-1,2k}^{n,\frac{h}{2}} + \phi_{2i-1,2j,2k-1}^{n,\frac{h}{2}} \\ &+ \phi_{2i-1,2j,2k}^{n,\frac{h}{2}} + \phi_{2i,2j-1,2k-1}^{n,\frac{h}{2}} + \phi_{2i,2j-1,2k}^{n,\frac{h}{2}} + \phi_{2i,2j,2k-1}^{n,\frac{h}{2}} + \phi_{2i,2j,2k}^{n,\frac{h}{2}}\Big)\Big|. \end{aligned}$$

Here, $\phi_{ijk}^{n,h}$ refers to ϕ_{ijk}^n with the space step h and $\phi_{ijk}^{n,\frac{h}{2}}$ refers to ϕ_{ijk}^n with the space step $\frac{h}{2}$. The rate of convergence is examined by the following ratio:

$$\log_2\left(\frac{\|e^{h,\frac{h}{2}}\|_2}{\|e^{\frac{h}{2},\frac{h}{4}}\|_2}\right).$$

The errors and rates of convergence are illustrated in Table 1. The results show that the scheme for both the phase-field ϕ and the temperature field U are second-order accurate in space.

For the following step, we present the convergence test of the Crank–Nicolson type scheme for both phase-field ϕ and temperature field U in time. We define the discrete

Table 1: Convergence rates with respect to the mesh sizes.

	Case	16-32	Rate	32-64	Rate	64-128
ϕ	l_2-error	7.959e-04	1.973	2.028e-04	1.979	5.144e-05
U	l_2-error	3.984e-04	1.973	1.015e-04	1.980	2.574e-05

l_2-norm of error to the time as

$$\left\|e^{\Delta t,\Delta t_{ref}}\right\|_2 = \sqrt{\frac{1}{N_h^3}\sum_{i,j,k}\left(e_{ijk}^{\Delta t,\Delta t_{ref}}\right)^2}, \tag{4.2}$$

where $e_{ijk}^{\Delta t,\Delta t_{ref}}$ is an absolute error between two numerical solutions defined as

$$e_{ijk}^{\Delta t,\Delta t_{ref}} = \left|\phi^{n,\Delta t} - \phi^{n,\Delta t_{ref}}\right|,$$

where $\phi^{n,\Delta t}$ is ϕ^n with the time step Δt, and $\phi^{n,\Delta t_{ref}}$ is that with the reference time step Δt_{ref}. To demonstrate the convergence rates in time, we fix the mesh size.

Tables 2 list the numerical convergence rates of Crank-Nicolson type scheme with respect to time step size Δt at $T = 64\Delta t_{ref}$, and the reference time step is $\Delta t_{ref} = 0.0125h^2$, where $h = \frac{100}{128}$, $\Delta t = 4\Delta t_{ref}, 8\Delta t_{ref}, 16\Delta t_{ref}$ are used in this test.

Table 2: Convergence rates with respect to time step sizes at the final time $T = 64\Delta t_{ref}$.

	Δt	$4\Delta t_{ref}$	Rate	$8\Delta t_{ref}$	Rate	$16\Delta t_{ref}$
ϕ	l_2-error	1.41e-05	2.1615	6.31e-05	2.1568	2.814e-04
U	l_2-error	1.47e-05	2.0688	6.18e-05	2.0029	2.475e-04

Now, we consider the convergence analysis for parameters h and λ. Let us consider a spherical ice in three-dimensional domain $\Omega = (-50, 50)^3$. We use parameters such as $N = N_x = N_y = N_z = 64, 128, 256$ and $\epsilon = \epsilon_3, \epsilon_6, \epsilon_{12}$, respectively. $M = 0.1, h = \frac{100}{N_x}$, $\Delta t = 0.05h^2$. In this test, $U \equiv 1$ are used. Then, the governing equation (2.6) becomes

$$\frac{\partial \phi}{\partial t} = M\left(\Delta\phi - \frac{F'(\phi)}{\epsilon^2}\right) - \lambda\frac{\sqrt{2F(\phi)}}{\epsilon}. \tag{4.3}$$

The initial condition is

$$\phi(x, y, z, 0) = \tanh\left(\frac{R_0 - R}{\sqrt{2}\epsilon}\right),$$

where $R = \sqrt{x^2 + y^2 + z^2}$ and the initial radius $R_0 = 35$. Then, the theoretical radius at time t is given as $R_T(t) = R_0 - \lambda t$. We select $\lambda = 0, 5$ and change N. Figs. 4(a), 4(b), and 4(c) show the results with $N = 64, 128$, and 256, respectively. We can observe that the numerical solutions are consistent with the theoretical values when $N = 128$ and 256, i.e., the numerical solution with the grid size $N = 128$ is accurate enough. Therefore, from now on, we will use $N = 128$ for the following tests.

Fig. 5 shows the temporal evolution of the spherical melting ice. Here, we set $N = 128, \lambda = 5, \epsilon = \epsilon_6$, and $M = 0.1$. Figs. 5(a), 5(b), and 5(c) are the results with the radius of sphere $R = 35, 21.7594$, and 15.4966, respectively.

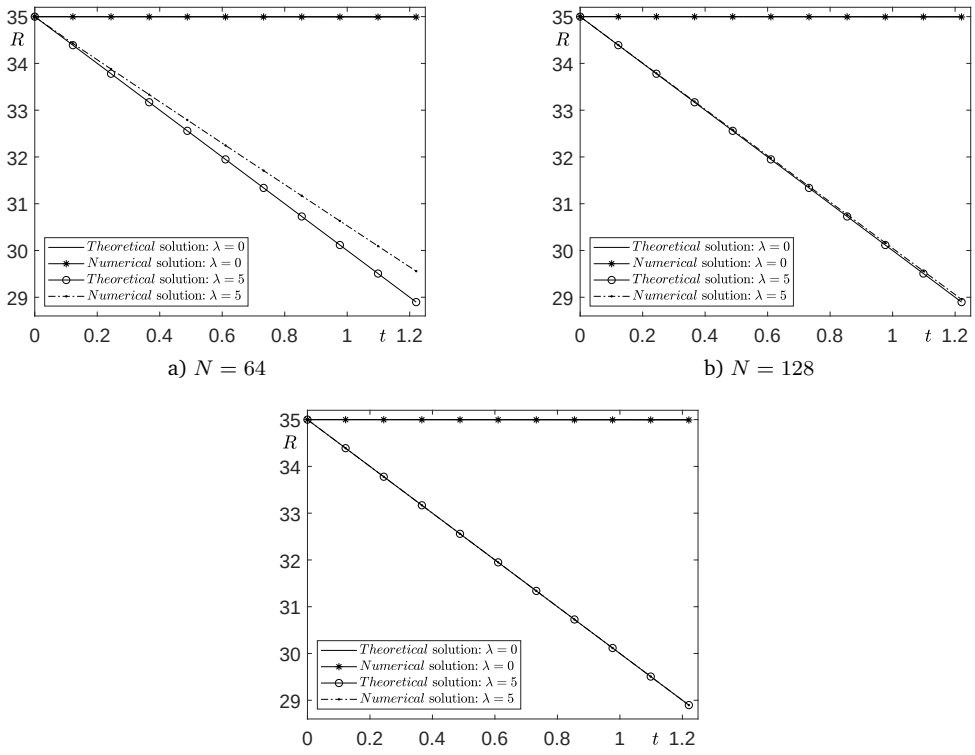

a) $N = 64$ b) $N = 128$

c) $N = 256$

Figure 4: Convergence test for grid size.

a) $t = 0$ b) $t = 100\Delta t$ c) $t = 200\Delta t$

Figure 5: Temporal evolution of a spherical melting ice.

4.2. Physical validation of model through Stefan problem

We conduct the numerical simulation in order to verify the physical validity of our model in this section. We implement a system that applies the Stefan condition into the phase-field model [4], which is

$$\frac{\partial U}{\partial t} = \Delta U - \frac{1}{2}\frac{\partial \phi}{\partial t}, \tag{4.4}$$

$$\left(\bar{\alpha}+\frac{5}{12}\bar{\varepsilon}\right)\frac{\partial\phi}{\partial t}=\Delta\phi+\frac{1}{\varepsilon^2}\big(2\phi+\bar{\varepsilon}U\big)\big(1-\phi^2\big), \tag{4.5}$$

where $\bar{\alpha}$ represents the strength of kinetic undercooling, $\bar{\varepsilon}$, ε are dimensionless constants which represent the thickness of interfacial region ϵ in [4]. We solve Eqs. (4.4) and (4.5) numerically using our second-order finite difference discretization scheme. Though Eqs. (4.4) and (4.5) are the solidification model that is physically different from the melting process we have presented in this paper, however the temporal behavior of phase-field that appears when applying the Stefan condition is topologically the same of ours since the interface moves towards the area of low temperature. Fig. 6 shows the phase-field and the temperature field with analytic solution given by [4].

A three-dimensional sphere is adopted as a computational domain using spherically symmetric scheme on $|x|\in(0,L)$ with an initial radius $R_0=0.2$. Parameters are appropriately scaled based on the reference [4]; $h=\frac{2}{1024}$, $d=0.001$, $\Delta t=100h^2$, $\bar{\alpha}=20$, $\varepsilon=0.01$, $\bar{\varepsilon}=10$. We employ $L=2$ and calculate the solution from time $t_0=4$. The homogeneous Neumann boundary condition is employed to the phase-field $\phi(x,t)$ while mixed boundary conditions are employed to the temperature field $U(x,t)$ as follows:

$$\frac{\partial U}{\partial x}(0,t)=0,\quad \frac{\partial U}{\partial x}(L,t)=-\frac{\gamma}{L}(U-U_\infty),$$

where $\gamma=0.05$ in this test. Here, a positive constant γ plays a role in motion of interface and corresponds to the far field condition $U_\infty\approx-0.0046$. Note that analytic solutions are provided in [4] as follows:

$$\Gamma(t)=\Big\{x\big||x|=R(t)=2\gamma\sqrt{t}\Big\}, \tag{4.6}$$

$$U(x,t)=-\frac{2d(1+\bar{\alpha}\gamma^2)\mathrm{erf}(|x|/\sqrt{4t})}{\mathrm{erf}(\gamma)|x|}-\int_\gamma^{\max(\gamma,|x|/\sqrt{4t})}\frac{2\gamma^3e^{\gamma^2-y^2}}{y^2}dy, \tag{4.7}$$

where Γ is an interface, $\mathrm{erf}(\cdot)$ is an error function. We omit the details and refer interested readers to the elaborate physical interpretation of [4] and the references therein.

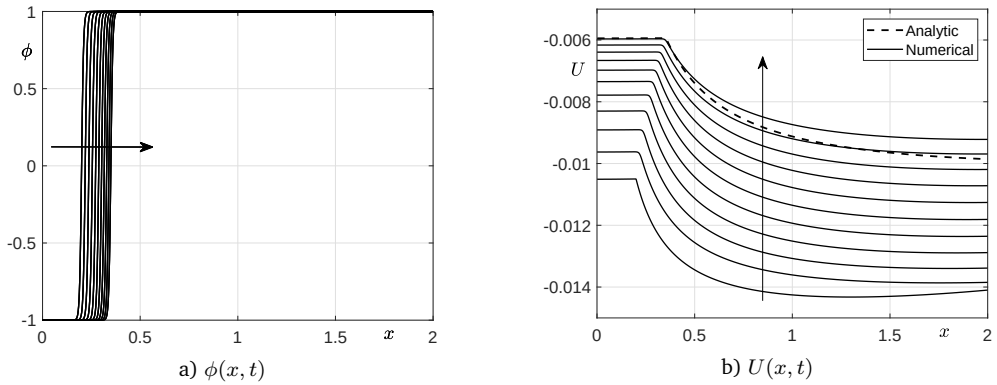

a) $\phi(x,t)$ b) $U(x,t)$

Figure 6: a) Temporal evolutions of phase-field of the solidification model with Stefan condition. b) Corresponding temperature field and its analytic solution. Note that the final time is $T\approx12.5$.

According to Fig. 6, the corresponding model with our proposed scheme interprets the motion of interface well and the temperature field as well as the analytic solution of this model. Therefore, a kind of systems of phase-field model related equations (4.4) and (4.5) via our proposed second-order method can be applied to the melting physics indeed.

4.3. Numerical simulation for ice melting

From now on, we consider the full governing equations (2.6) and (2.7). We consider an ice cube with the length of 1.2 is in the center of the domain $\Omega = (-50, 50)^3$. We set $\phi(x, y, z, 0) = 1$ and $\phi(x, y, z, 0) = -1$ for the ice cube and water, respectively. The initial condition of temperature is given as

$$U(x, y, z) = \begin{cases} 0, & \text{if} \quad \phi(x, y, z, 0) = 1, \\ 1, & \text{otherwise.} \end{cases}$$

We use $N = 128, h = 100/N, \Delta t = 0.05h^2, \epsilon = \epsilon_6, \lambda = 5, D = 1$, and $M = 10\epsilon$ for the numerical experiment. Fig. 7 shows the temporal evolution of the ice melting. The ice cube melts due to heat from the surrounding water.

Then, we verify the energy dissipation of the proposed model. We define the discrete energy functional as

$$\begin{aligned} \mathscr{W}_d(\phi^n) = \frac{hM}{2} \sum_{i=1}^{N_x-1} \sum_{j=1}^{N_y-1} \sum_{k=1}^{N_z-1} \left((\phi^n_{i+1,jk} - \phi^n_{ijk})^2 + (\phi^n_{i,j+1,k} - \phi^n_{ijk})^2 + (\phi^n_{ij,k+1} - \phi^n_{ijk})^2 \right) \\ + h^3 \sum_{i=1}^{N_x} \sum_{j=1}^{N_y} \sum_{k=1}^{N_z} \left(M \frac{F(\phi^n_{ijk})}{\epsilon^2} + \frac{\lambda U^n_{ijk}}{\sqrt{2}\epsilon} \left(\phi^n_{ijk} - \frac{1}{3} (\phi^n_{ijk})^3 \right) \right). \end{aligned}$$

As shown in Fig. 8, we see that the energy decreases with the increasing number of iterations until it stabilizes.

Next, we consider another ice melting phenomenon. In this test, we verify whether the numerical results of the melting model are consistent with physical phenomenon.

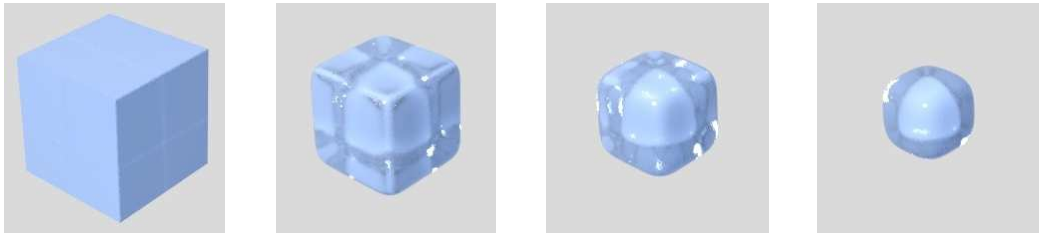

a) $t = 0$ b) $t = 50\Delta t$ c) $t = 100\Delta t$ d) $t = 150\Delta t$

Figure 7: Melting process of an ice cube.

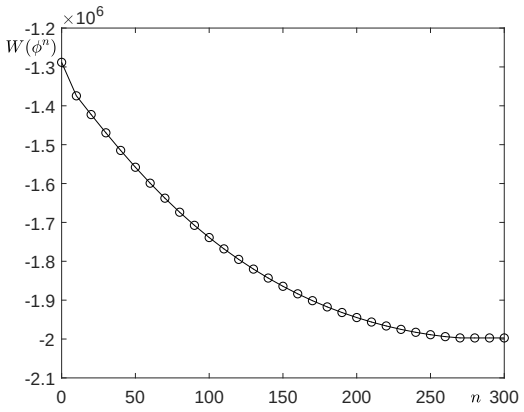

Figure 8: Energy dissipation of ice cube model.

We study the effect of the contact area between ice and water on the water temperature. We consider two ice cubes with different surface areas. A schematic diagram of an ice cube with a hole is shown in Fig. 9. At the center of the ice cube, there is a hollow cylinder. We denote the lengths of the cube's x-, y-, z-axis edges by L_x, L_y, L_z, respectively, and the initial radius of the hollow cylinder by R_0.

We consider two cubes with different initial radius: a cube with radius $R_0 = 15$ (cube 1) and the other one with radius $R_0 = 20$ (cube 2) as shown in Fig. 10(a) and Fig. 11(a), respectively. We set the same parameters: $L_x = L_y = L_z = 60, N = 128, h = \frac{100}{N}, \Delta t = 0.05h^2, \epsilon = \epsilon_6, \lambda = 5, D = 1$, and $M = 10\epsilon$.

We define the volumes of ice and water as

$$V_{ice}^n = \sum_{i=1}^{Nx}\sum_{j=1}^{Ny}\sum_{k=1}^{Nz}\frac{h^3}{2}\big(1+\phi_{ijk}^n\big), \quad V_{water}^n = \sum_{i=1}^{Nx}\sum_{j=1}^{Ny}\sum_{k=1}^{Nz}\frac{h^3}{2}\big(1-\phi_{ijk}^n\big). \tag{4.8}$$

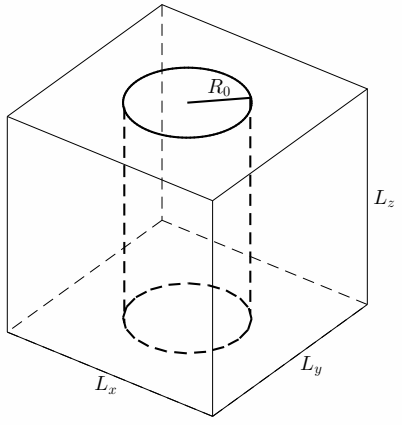

Figure 9: Schematic diagram of ice cube.

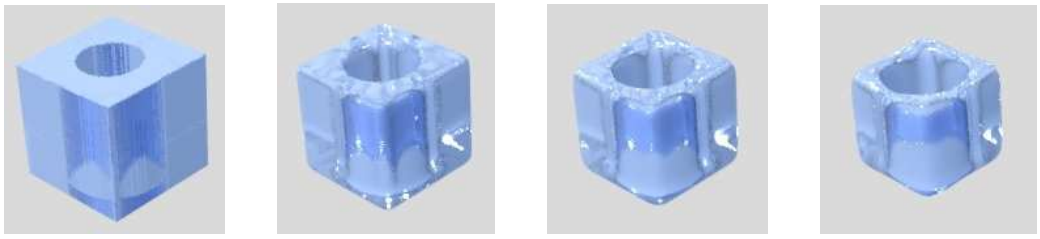

a) $t = 0$ b) $t = 15\Delta t$ c) $t = 30\Delta t$ d) $t = 50\Delta t$

Figure 10: Melting process of ice cube with $R_0 = 15$.

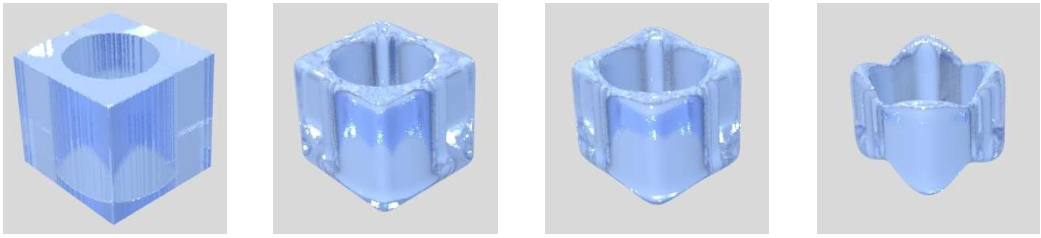

a) $t = 0$ b) $t = 15\Delta t$ c) $t = 30\Delta t$ d) $t = 50\Delta t$

Figure 11: Melting process of ice cube with $R_0 = 20$.

We set a formula

$$U_{ave}^n = \frac{1}{V_{water}^n} \sum_{i=1}^{Nx} \sum_{j=1}^{Ny} \sum_{k=1}^{Nz} U_{ijk}^n \frac{h^3}{2} (1 - \phi_{ijk}^n) \tag{4.9}$$

to check the changing trend of water temperature as shown in Fig. 12(a).

From the numerical solutions, we see that the water temperature of both cube 1 and cube 2 drop at first, then temperature of the water increase to the initial values of water. We see that the water with cube 2 first returned to the initial value of water

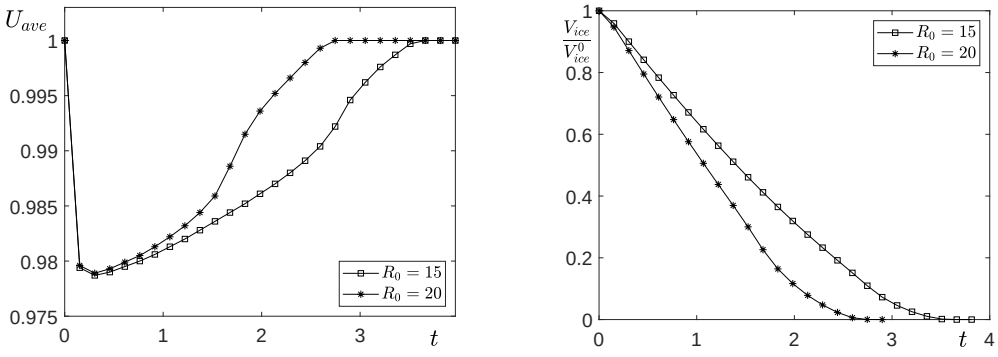

a) Temperature change of water b) Volume change of ice cube

Figure 12: Changing process of water temperature and ice volume.

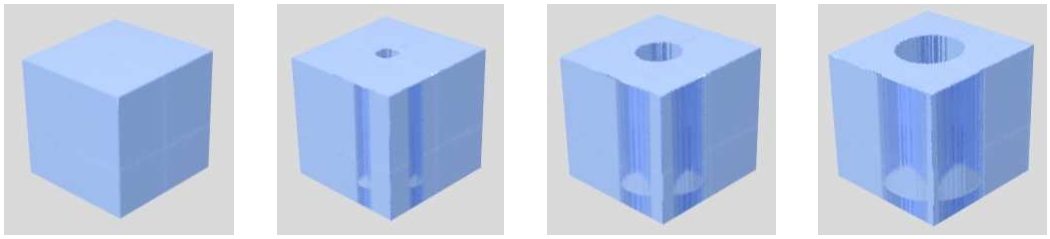

a) V_1 b) V_2 c) V_3 d) V_4

Figure 13: Initial cube shape.

temperature than the water with cube 1. Besides, as shown in Fig. 12(b), cube 2 melts faster than cube 1, which indicates that a cube with a larger surface melts faster. Here, we define the complete melting if $V_{ice}^n/V_{ice}^0 < \eta$ for some small η. We set $\eta = 0.005$.

Now, we select four ice cubes with the same volume and different shapes: V_1, V_2, V_3, and V_4 as shown in Fig. 13. Let the length of the cube $L_x = L_y = L_z = l$ and the volume of the cube be V_0. We define

$$V_0 = L_x L_y L_z - L_z \pi R_0^2, \tag{4.10}$$

and

$$\phi(x, y, z, 0) = \begin{cases} 1, & \text{if} \quad \sqrt{x^2 + y^2} - R_0 < 0, \\ -1, & \text{otherwise.} \end{cases}$$

We denote the surface area of the cube by S. The parameters used are listed in Table 3.

Table 3: Parameter values of ice cubes.

Shape	V_1	V_2	V_3	V_4
l	60.000	60.435	61.745	63.920
R_0	0	5	10	15
V_0	216000	216000	216000	216000
S	21600	23656	26126	29125

The changing trend of water temperature is shown in Fig. 14(a) and the volume changing process of ice cube is shown in Fig. 14(b). Times for four ice cubes, V_1, V_2, V_3, and V_4, to melt completely are $280\Delta t, 270\Delta t, 170\Delta t$, and $140\Delta t$, respectively. From this test, we can conclude that the water temperature of all the four cubes drop at first, then temperature of the water increase to the initial values of water. Besides, the water with cube which has a larger surface first returned to the initial value of water temperature, and under the same volume, the ice cube melts faster if it has a larger surface area.

Next, we perform the melting of many cubes in a cup which is full of water, and we set the parameters such as $\Omega = (-50, 50)^3, N = 128, h = \frac{100}{N}, \Delta t = 0.05h^2, \epsilon = \epsilon_6, \lambda = 5, D = 1$, and $M = 10\epsilon$. The temporal evolution of the ice cubes is shown in Fig. 15.

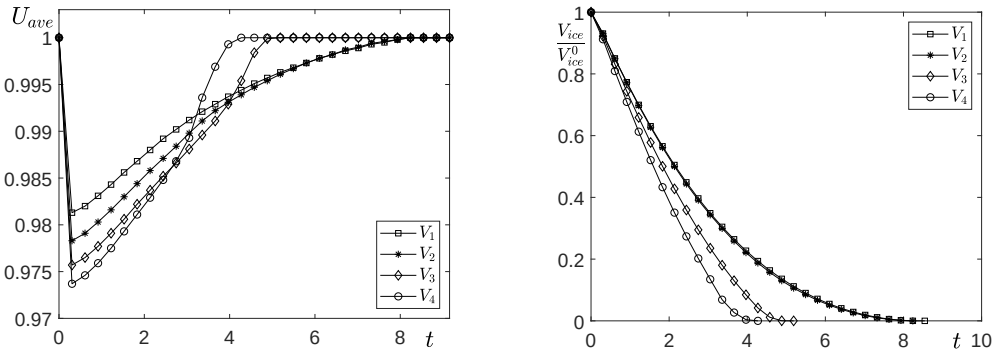

a) Temperature change of water b) Volume change of ice cube

Figure 14: Changing process of water temperature and ice volume.

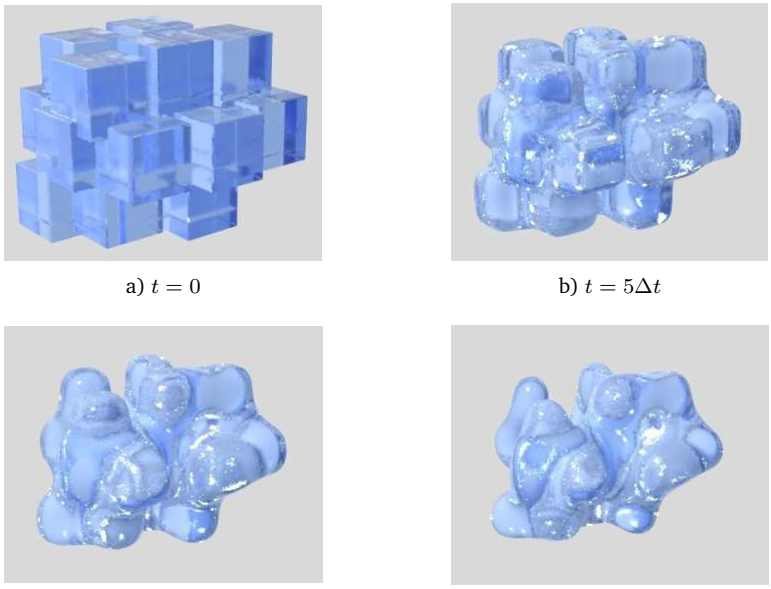

a) $t = 0$ b) $t = 5\Delta t$

c) $t = 10\Delta t$ d) $t = 15\Delta t$

Figure 15: Melting process of many ice cubes.

4.4. Complex ice melting

In this section, we consider ice melting of complex shapes such as Armadillo and Dragon models in three-dimensional space $\Omega = (-50, 50)^3$. We set the parameters of two models as $N = 128, h = \frac{100}{N}, \Delta t = 0.05h^2, \epsilon = \epsilon_6, \lambda = 5, D = 1$, and $M = 10\epsilon$. Figs. 16(a) and 16(e) show the initial state of two models. Fig. 16 shows the melting states of Armadillo and Dragon models at $t = 5\Delta t, 10\Delta t$, and $15\Delta t$.

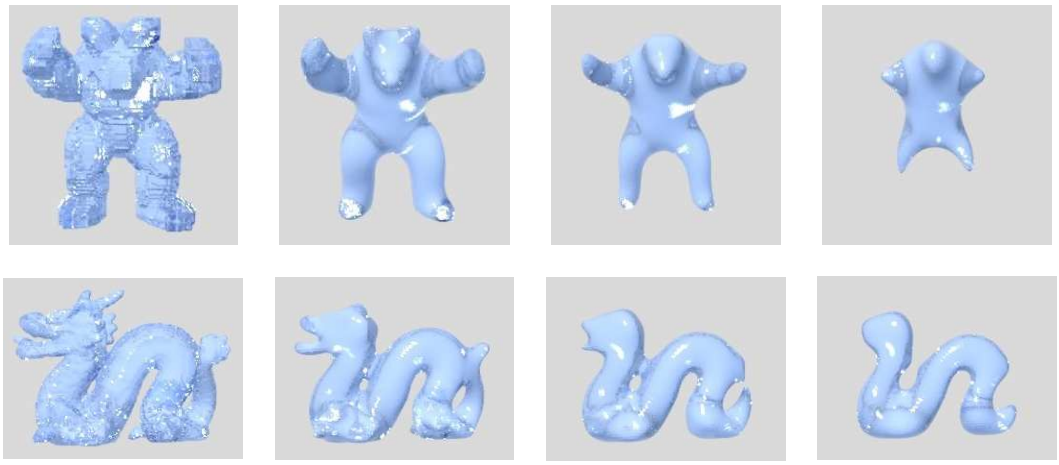

a) $t = 0$ b) $t = 5\Delta t$ c) $t = 10\Delta t$ d) $t = 15\Delta t$

Figure 16: Melting process of complex models.

5. Conclusion

In this paper, we proposed the mathematical model based on the phase-field modeling for the crystal growth and presented numerical simulations for ice melting phenomena. To model ice melting, we ignore anisotropy in the crystal growth model and add a melting term. The proposed numerical solution algorithm is a hybrid method which uses both the analytical and numerical solutions. By performing various computational experiments, we confirmed the accuracy and efficiency of the proposed method for ice melting. We also verified a cube which has a larger contact area with the surrounding water makes the water temperature drop faster, and under the same volume, a cube melts faster if it has a larger surface area. The numerical results of the melting model were consistent with the physical phenomena.

In addition, as an interesting topic, visual simulation of ice has been widely researched in the field of computer graphics. A benchmark such as the dragon was taken for simulating ice melting in computer graphics [15, 26]. While comparing via visual, ice melting phenomenon is achieved similarly with our proposed method. Because we focused on the mathematical modeling and numerical simulations for ice melting in this paper, we leave the analysis of the proposed model in future work.

Acknowledgments

The first author (Jian Wang) was supported by the China Scholarship Council (201808260026). The author (H. G. Lee) was supported by Basic Science Research Program through the National Research Foundation of Korea (NRF) funded by the Ministry of Education (NRF-2019R1C1C1011112). The corresponding author (J.S. Kim) was supported by Basic Science Research Program through the National Research Founda-

tion of Korea (NRF) funded by the Ministry of Education (NRF-2019R1A2C1003053). The authors would like to thank the reviewers for their constructive and helpful comments on the revision of this article.

References

[1] S. M. Allen and J. W. Cahn, *A microscopic theory for antiphase boundary motion and its application to antiphase domain coarsening*, Acta Metall., 27 (1979), 1085–1095.
[2] W. L. Briggs, *A Multigrid Tutorial*, SIAM, 1987.
[3] G. Caginalp, *Stefan and Hele–Shaw type models as asymptotic limits of the phase-field equations*, Phys. Rev. A, 39 (1989), 5887–5896.
[4] G. Caginalp, X. Chen, C. Eck, *Numerical tests of a phase field model with second order accuracy*, SIAM J. Appl. Math., 68(6) (2008), 1518–1534.
[5] M. Carlson, P. Mucha, B. V. H. Iii and G. Turk, *Melting and flowing*, In Proc. ACM SIGGRAPH Symposium on Comput. Animat., (2002), 167–174.
[6] H. D. Ceniceros, R. L. Nos and A. M. Roma, *Three-dimensional, fully adaptive simulations of phase-field fluid models*, J. Comput. Phys., 229 (2010), 6135–6155.
[7] C. C. Chen and C. W. Lan, *Efficient adaptive three-dimensional phase-field simulation of dendritic crystal growth from various supercoolings using rescaling*, J. Cryst. Growth., 311 (2009), 702–706.
[8] J. M. Church, Z. Guo, P. K. Jimack, A. Madzvamuse, K. Promislow, B. Wetton, S. M. Wise and F. Yang, *High accuracy benchmark problems for Allen–Cahn and Cahn–Hilliard dynamics*, Commun. Comput. Phys., 26 (2019), 947–972.
[9] E. V. L. de Mello and O. Teixeira da Silveira Filho, *Numerical study of the Cahn–Hilliard equation in one, two and three dimensions*, Phys. A, 347 (2005), 429–443.
[10] I. W. Eames and K. T. Adref, *Freezing and melting of water in spherical enclosures of the type used in thermal (ice) storage systems*, Appl. Therm. Eng., 22 (2002), 733–745.
[11] J. J. Eggleston, G. B. McFadden and P. W. Voorhees, *A phase-field model for highly anisotropic interfacial energy*, Phys. D, 150 (2001), 91–103.
[12] M. Fujisawa and K. T. Miura, *Animation of ice melting phenomenon based on thermodynamics with thermal radiation*, In Proc. GRAPHITE, (2007), 249–256.
[13] I. Fujishiro and E. Aoki, *Volume graphics modeling of ice thawing*, Vol. Graph., (2001), 69–80.
[14] Y. Guo, H. Zhang, W. Yang, J. Wang, and S. Song, *A high order operator splitting method for the degasperis-procesi equation*, Numer. Math. Theor. Meth. Appl., 12(3) (2019), 884–905.
[15] K. Iwasaki, H. Uchida, Y. Dobashi and T. Nishita, *Fast particle-based visual simulation of ice melting*, Comput. Graph. Forum, 29 (2010), 2215–2223.
[16] D. Jacqmin, *Calculation of two-phase Navier–Stokes flows using phase-field modeling*, J. Comput. Phys., 155 (1999), 96–127.
[17] D. Jeong, Y. Li, C. Lee, J. Yang, J. Kim, *A conservative numerical method for the Cahn–Hilliard equation with generalized mobilities on curved surfaces in three-dimensional space*, Commun. Comput. Phys., 27(2) (2020), 412–430.
[18] J. H. Jeong, N. Goldenfeld and J. A. Dantzig, *Phase field model for three-dimensional dendritic growth with fluid flow*, Phys. Rev. E, 64 (2001), 041602.
[19] M. W. Jones, *Melting objects*, The J. WSCG, 11 (2003), 247–254.

[20] R. KEISER, B. ADAMS, D. GASSER, P. BAZZI, P. DUTRE AND K. GROSS, *A unified lagrangian approach to solidfluid animation*, In Proc. Eurographics Symposium on Point-Based Graphics, (2005), 125–133.
[21] J. KIM, *Phase-field models for multi-component fluid flows*, Commun. Comput. Phys., 12 (2012), 613–661.
[22] Y. T. KIM, *Computational Studies of Dendritic Crystal Growth*, Ph.D. Thesis, University of Illinois at Urbana-Champaign, 2003.
[23] H. G. LEE AND J. KIM, *Regularized Dirac delta functions for phase field models*, Int. J. Numer. Methods Eng., 91(3) (2012), 269–288.
[24] G. L. LEI, W. DONG, M. ZHENG, Z. Q. GUO AND Y. Z. LIU, *Numerical investigation on heat transfer and melting process of ice with different porosities*, Int. J. Heat Mass Transf., 107 (2017), 934–944.
[25] Y. LI, H. G. LEE AND J. KIM, *A fast, robust, and accurate operator splitting method for phase-field simulations of crystal growth*, J. Cryst. Growth, 321 (2011), 176–182.
[26] S. Y. LII AND S. K. WONG, *Ice melting simulation with water flow handling*, Vis. Comput., 30 (2014), 531–538.
[27] H. LIU AND S. LEUNG, *A simple semi-implicit scheme for partial differential equations with obstacle constraints*, Numer. Math. Theor. Meth. Appl., 13(3) (2020), 620–643.
[28] F. LOSASSO, G. IRVING, E. GUENDELMAN AND R. FEDKIW, *Melting and burning solids into liquids and gases*, IEEE Trans. Vis. Comput. Graph., 12 (2006), 343–352.
[29] L. MA, R. CHEN, X. YANG AND H. ZHANG, *Numerical approximations for Allen–Cahn type phase field model of two-phase incompressible fluids with moving contact lines*, Commun. Comput. Phys., 21 (2017), 867–889.
[30] Q. MIAO, *Eigenvalues for a Neumann boundary problem involving the $p(x)$-Laplacian*, Adv. Math. Phys., Vol. 2015, 2015.
[31] M. MÜLLER, R. KEISER, A. NEALEN, M. PAULY, M. GROSS AND M. ALEXA, *Point based animation of elastic, plastic and melting objects*, In Proc. ACM Comput. Animat., (2004), 141–151.
[32] A. PAIVA, F. PETRONETTO, T. LEWINER AND G. TAVARES, *Particle-based non-Newtonian fluid animation for melting objects*, In Proc. SIBGRAPI., (2006), 78–85.
[33] R. S. QIN AND H. K. BHADESHIA, *Phase field method*, Mater. Sci. Technol., 26(7) (2010), 803–811.
[34] J. C. RAMIREZ, C. BECKERMANN, A. KARMAA AND H. J. DIEPERS, *Phase-field modeling of binary alloy solidification with coupled heat and solute diffusion*, Phys. Rev. E, 69 (2004), 051607.
[35] H. L. REN, X. Y. ZHUANG, C. ANITESCU AND T. RABCZUK, *An explicit phase field method for brittle dynamic fracture*, Comput. Struct., 217 (2019), 45–56.
[36] J. SHIN, H. G. LEE AND J. Y. LEE, *First and second order numerical methods based on a new convex splitting for phase-field crystal equation*, J. Comput. Phys., 327 (2016), 519–542.
[37] J. SHIN, H. G. LEE AND J. Y. LEE, *Convex splitting Runge–Kutta methods for phase-field models*, Comput. Math. Appl., 73(11) (2017), 2388–2403.
[38] B. SOLENTHALER, J. SCHLAFLI AND R. PAJAROLA, *A unified particle model for fluid-solid interactions*, Comput. Animat. Virtual Worlds, 18 (2007), 69–82.
[39] M. SUGAWARA, Y. KOMATSU AND H. BEER, *Three-dimensional melting of ice around a liquid-carrying tube*, Heat Mass Transf., 47 (2011), 139–145.
[40] D. TERZOPULOS, J. PLATT AND K. FLEISCHER, *Heating and melting deformable models (from goop to glop)*, In Proc. Graphics Interface, 89 (1989), 219–226.
[41] D. TONNSEN, *Modeling liquids and solids using thermal particles*, In Proc. Graphics Inter-

face, (1991), 255–262.
[42] U. TROTTENBERG, C. OOSTERLEE AND A. SCHULLER, *Multigrid*, Academic Press London, 2001.
[43] P. VIGNAL, L. DALCIN, D. L. BROWN, N. COLLIER AND V. M. CALO, *An energy-stable convex splitting for the phase-field crystal equation*, Comput. Struct., 158 (2015), 355–368.
[44] J. WANG, Y. LI, Y. CHOI, C. LEE AND J. KIM, *Fast and accurate smoothing method using a modified allen–cahn equation*, Comput. Aided Des., 120 (2020) 102804.
[45] C. WOJTAN, M. CARLSON, P. J. MUCHA AND G. TURK, *Animating corrosion and erosion*, In Eurographics Workshop on natural phenom, (2007), 15–22.
[46] C. YANG, Q. XU AND B. LIU, *GPU-accelerated three-dimensional phase-field simulation of dendrite growth in a nickel-based superalloy*, Comput. Mater. Sci., 136 (2017), 133–143.
[47] J. YANG AND J. KIM, *An unconditionally stable second-order accurate method for systems of Cahn–Hilliard equations*, Commun. Nonlinear Sci. Numer. Simul., 87 (2020), 105276.
[48] Y. ZHAO, L. WANG, F. QIU, A. KAUFMAN AND K. MUELLER, *Melting and flowing in multi-phase environment*, Comput. Graph., 30 (2006), 519–528.
[49] L. ZHENG, M. YANG AND Y. ZHANG, *Numerical simulation of melting problems using the-lattice Boltzmann method with the interfacial tracking method*, Numer. Heat Transfer A, 68 (2015), 1175–1197.